Guiding, Focusing, and Collimated Transport of Hot Electrons in a Canal in the Extended Tip of Cone Targets

N. Renard-Le Galloudec,[1] E. d'Humières,[1,3] B. I. Cho,[2] J. Osterholz,[2,4] Y. Sentoku,[1] and T. Ditmire[2]

[1]*Nevada Terawatt Facility, Department of Physics, University of Nevada, Reno, Nevada 89521-0042, USA*

[2]*Texas Center for High Intensity Laser Science, Department of Physics, University of Texas, Austin, Texas 78712-0263, USA*

[3]*Centre Lasers Intenses et Applications, UMR 5107, Université de Bordeaux - CNRS - CEA, 33405 Talence, France*

[4]*Institute of Laser and Plasmaphysics, Heinrich-Heine-University, Gebaeude 25.33, Universitaetsstraße 1, 40225, Duesseldorf, Germany*

(Received 3 October 2008; published 20 May 2009)

Hot electrons are produced, guided into a beam, and transported over 60 μm in a small canal to the outside tip of a structured cone target. The diameter of the electron beam is defined by the inside tip diameter. This carries the potential to create electron beams of specific diameters propagating over specific distances of interest for several applications.

DOI: 10.1103/PhysRevLett.102.205003 PACS numbers: 52.57.Bc, 52.25.Fi, 52.65.Rr

The interaction of high intensity short-pulse lasers with conical targets has been of increasing interest in recent years. The most studied application is fast ignition [1–15]. In a cone target, the laser light is optically guided by the conical geometry and focuses at the tip [8]. When a sufficient magnetic field is generated along the surface, a significant fraction of the electrons is guided toward the tip [8,14]. These processes increase the energy density and particle fluxes in the tip of the cone making this area relevant for not only fast ignition [1–14,16] but also stockpile stewardship, radiative properties and equations of state, laboratory astrophysics [15,17], enhanced backlighters [18–20], and medical applications [21,22]. Recent studies have investigated the effect of the cone angle and f number of the focusing optic, the ratio of the laser spot size to the cone tip size [2,13,23], preplasma filling inhibition of fast electron energy deposition [24,25], and deeper propagation and energy deposition into the cone at higher contrast [26]. It has also been suggested that target structure can collimate fast electrons [27]. The data presented here show that, under the right conditions, the electrons are guided into the tip where they form a beam equal to the inside tip diameter. In addition, due to the presence of a canal in the tip, we see collimated transport of this beam over 60 μm to the outside tip where the coherent transition of radiation (CTR) is emitted [28,29]. Such a target, along with controlled irradiation, has the potential to obtain electron beams with specific characteristics.

The experiment was performed at the University of Texas, Austin, on the Texas High Intensity Optical Research laser with 0.7 J at 800 nm, 40 fs FWHM, 7 μm FWHM focal spot diameter, and 2×10^{19} W/cm^2 [30,31]. Typical cones were characterized with a scanning electron microscope (SEM) and systematically aligned to obtain reproducible parameters on target [31,32]. The best focus was aligned on axis at the base of the cone allowing the laser to diverge as it enters the cone, thus enlarging the irradiation diameter to 21 μm (and reducing the intensity to 10^{18} W/cm^2) before hitting the faces of the cone, mitigating preplasma issues [31]. We recorded 2D images of the 800 nm CTR light emitted on axis from the tip of the cone with a 2-inch diameter, 4-inch focal length achromat [32].

Figures 1(a) and 1(b) present SEM images of these extended tip copper cone targets. Figures 1(a) and 1(b) are, respectively, the top and side view of the 15–20 μm outer tip diameter. The dashed circle [Fig. 1(a)] and the dashed line [Fig. 1(b)] represent the diameter of the laser irradiation spot inside the cone. An inset in the bottom left corner of Fig. 1(a) shows a typical 5 by 5 μm FWHM of the 2D CTR emission from the outside tip of these cones. The filled solid circle in Fig. 1(a) and the filled solid rectangle in Fig. 1(b) represent the hot electron beam that produces the observed CTR signal. The dotted lines in Fig. 1(b) represent the inside faces of the cone to the inside tip. An inset magnifying the tip is shown at the bottom of Fig. 1(b). The solid black rectangle at the very tip of the cone represents the size of the CTR emitting zone. The dashed red lines represent the collection optic solid angle. The solid orange lines are perpendicular to these. The tip is quasiflat over a transversal dimension 3–4 times larger than the CTR emitting zone. Under these conditions, it seems reasonable to assume that the electrons are emitted from the extended tip at an angle close to the surface normal [33]. Consequently, the CTR is emitted within the collection angle of the imaging optic. Figure 1(c) shows the inside of the cone as the laser "sees" it. The dashed circle corresponds to the diameter of the laser irradiation spot inside the cone. Figure 1(d) has been taken at a higher magnification as far as possible into the tip. The smallest inside tip diameter we could measure is of the order of

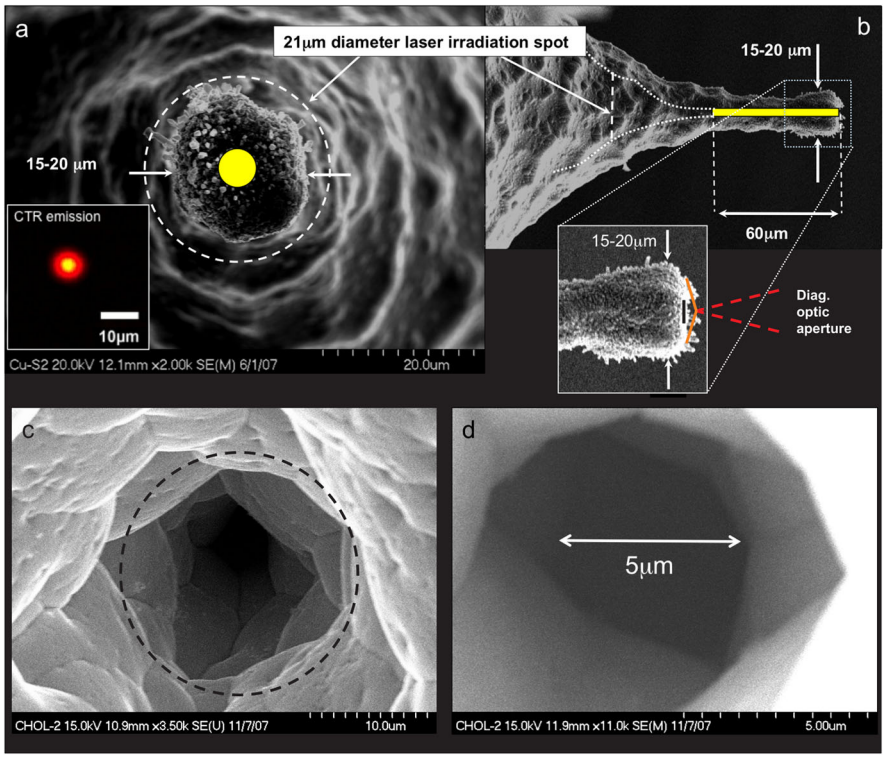

FIG. 1 (color online). SEM images of typical extended tip targets. (a), (b), (c), and (d) show, respectively, the outside tip of the target, the target side on, the inside tip of the target, and the same inside tip at a higher magnification.

5 μm. This is equal to the CTR emission diameter from the outside tip. We see in Fig. 1(b) that the hot electron beam propagated about 60 μm (from target metrology) from the inside tip to the outer tip of the cone. Figure 2 presents the horizontal and vertical FWHM of the CTR emission from a series of targets, including 10 μm thick flat targets. As we go from a flat target to cones of different characteristics, we see both the vertical and the horizontal diameter of the CTR emission become smaller and more reproducible. All cones had a blunt outside tip. The focus of this Letter is the third population, which has an *extended* tip compared to the rest. Bremsstrahlung x-ray measurements gave us a temperature of about 350 keV for both flat and cones in agreement with CTR emission from different thickness Al targets as explained in [32].

These targets built under contract by Nanolabz are entirely made of solid copper. The fabrication process does not involve any glue and thus increases the efficiency of

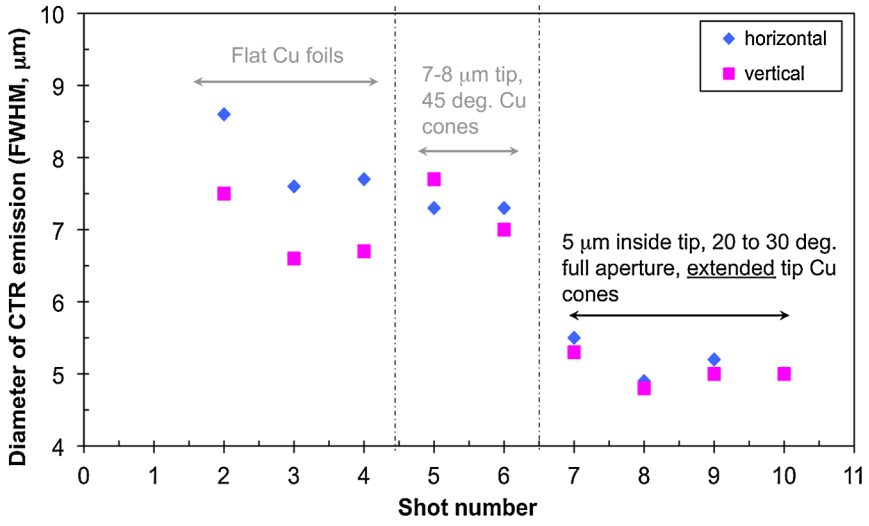

FIG. 2 (color online). Horizontal and vertical CTR emission (FWHM) as a function of target type.

our targets due to an enhanced electron transport mechanism [14]. Copper was deposited onto a thin silicon structure later etched away. Even though the deposition time was set to deposit 10 μm of copper, the shape of the target makes it possible for the thickness of the deposition to be slightly uneven along the target structure. For example, it is very likely that, at the base where the target is flat, the thickness is indeed 10 μm. On the sides of the cone closer to the tip, perpendicular to the base, it is likely that the deposited copper is thinner. Hence our outside measured diameter of 15–20 μm does not preclude a 5 μm or smaller diameter inside the canal.

We performed 2D collisionless particle-in-cell (PIC) simulations with the code PICLS to assess the electromagnetic field structure and hot electron transport in these cones. Collisionless PIC simulations investigate hot electron generation and transport and reveal most of the physics involved when the laser intensity is high enough for collisional effects to play a small role in electron transport [34]. In the simulations, the incident laser pulse has a 1 μm wavelength, a pulse duration of 40 fs, and a transverse spot size of 21 μm FWHM at 3×10^{18} W/cm^2 similar to the experiment [31]. The shape and thickness of the cone target in the simulations reproduces that shown in Fig. 1(b) with a 5 μm diameter inside tip continuing into a 5 μm inside diameter canal into the extended tip. The temporal and spatial (transverse) profiles are Gaussian, and the pulse is injected to the left of a 150×150 μm box. The laser interacts with the target at normal incidence, and its electric field is in the simulation plane (p polarization). The peak of the pulse enters the box 40 fs after the beginning of the calculation. So that the laser does not propagate inside the target, we set a target density 10 times higher than the relativistic critical density $a_0 n_c$, where a_0 is the normalized laser amplitude and n_c is the critical density [$n_c = 1.1 \times 10^{21}/\lambda\ (\mu\text{m})^2\,\text{cm}^{-3}$, λ is the laser wavelength]. The plasma, composed of Al ions and electrons, is initially fully ionized. The mesh size is $\Delta x = \Delta y =$ 80 nm with 5 aluminum ions and 65 electrons per cell. The target is initially cold (i.e., the initial electron temperature is zero) and the time step equal to 2.6×10^{-1} fs. The preplasma used in the simulation fills the cone funnel and has a constant density of $0.8 n_c$.

Figures 3(a)–3(c) show the 2D electron energy density for the funnel cone at 3×10^{18} W/cm^2, respectively, 132, 264, and 396 fs after the beginning of the calculations. The cone geometry increases the laser intensity from 3×10^{18} W/cm^2 to 2.2×10^{19} W/cm^2 at the inside tip. The laser transverse electrostatic field maximum amplitude is 4.6 TV/m before entering the cone. It reaches 12.7 TV/m at the cone inside tip (entrance of the cone funnel) and strongly decreases inside the funnel to 1.6 TV/m after propagating over one-third of the funnel length. The laser energy absorption is strongest at the inside tip of the cone where the laser is stopped by the high-density preplasma filling the funnel. That high electron energy density region (a signature of hot electron localization) shown in Fig. 3(b) is much smaller than the laser irradiation diameter of 21 μm and is equal to the diameter of the inside tip. Figure 3(c) shows that it preferentially propagates inside the canal and that, after several tens of microns of travel inside the canal, the hot electron beam is still narrower than the laser irradiation pattern. The 2D PIC simulations performed therefore indicate that the experimental observation of a CTR emission FWHM smaller than the laser pulse FWHM is due to the cone geometry and the structure of the extended tip. The temperature shown in Fig. 3 is calculated using the electron energy density and is a signature of the presence and localization of hot electrons. It is not a reliable indication of the background electron temperature at such an early time in the simulation (and even later in the simulation as binary collisions are not treated) [35].

We also performed two more simulations with different inside tip diameters prolonged into a canal of the same diameter as the tip. This demonstrates the crucial importance of the inside tip diameter in relation with the diameter of the hot electron beam. Figures 4(a)–4(c) show, respectively, a 2, 5, and 10 μm inside tip size. Strikingly, the hot electron beam diameter increases with the inside tip

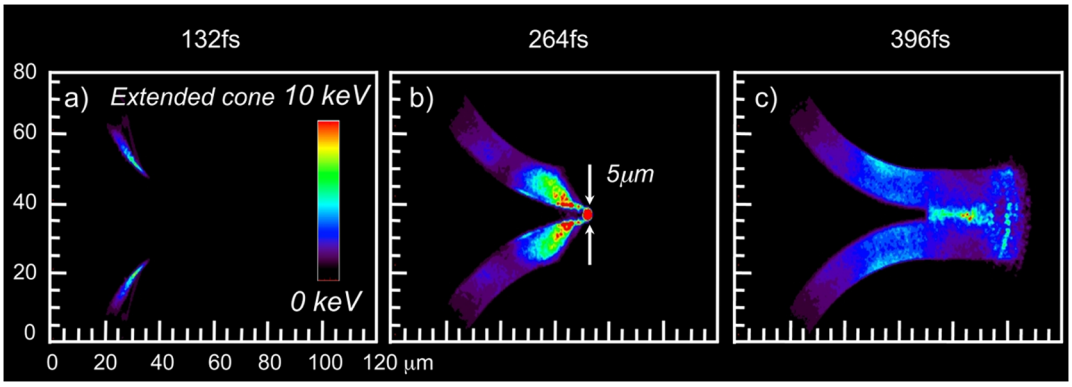

FIG. 3 (color online). (a), (b), and (c) show the 2D electron energy density for our cone target, respectively, 132, 264, and 396 fs after the beginning of the calculations.

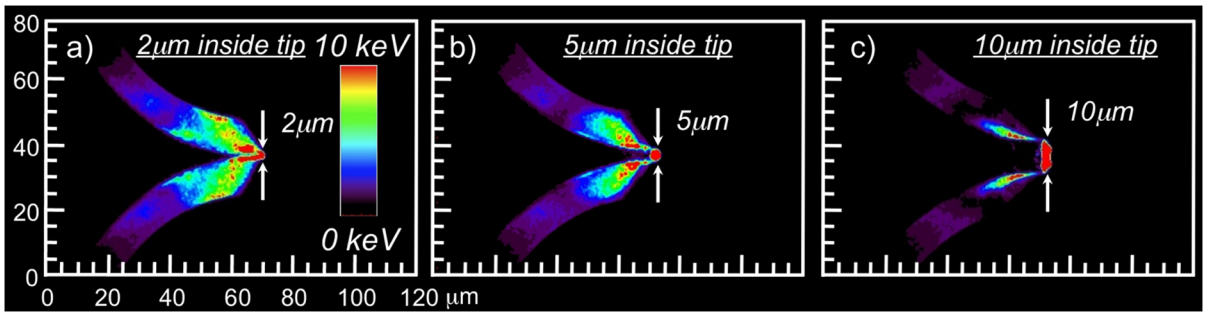

FIG. 4 (color online). (a), (b), and (c) show the electron energy density at 264 fs for, respectively, a 2, 5, and 10 μm diameter inside tip cone target.

(the canal entrance diameter) but remains small compared to the laser FWHM.

In conclusion, our data confirmed by simulations show the conical structure funnels the electrons into the tip of the cone. The beam being formed at the inside tip of the cone then travels into the canal inside the tip, to the end, over a distance of, in our case, 60 μm. Structuring the target could form and guide an electron beam of a specific diameter over specific distances. This opens the door to bigger tip sizes, which would increase the electron beam diameter available at the tip for applications such as fast ignition, equations of states, radiative properties, astrophysics, and enhanced backlighters.

This work was supported by the DOE Office of Fusion Energy Science under the Fusion Science Center and the National Nuclear Security Administration under cooperative Agreement No. DE-FC52-03NA00156.

[1] Y. Sentoku *et al.*, Phys. Plasmas **11**, 3083 (2004).
[2] M. Nakatsutsumi *et al.*, Phys. Plasmas **14**, 050701 (2007).
[3] Max Tabak *et al.*, Phys. Plasmas **1**, 1626 (1994).
[4] P. A. Norreys *et al.*, Phys. Plasmas **7**, 3721 (2000).
[5] M. Key, Nature (London) **412**, 775 (2001).
[6] R. Kodama *et al.*, Phys. Plasmas **8**, 2268 (2001).
[7] M. Key, Phys. Plasmas **14**, 055502 (2007).
[8] K. A. Tanaka *et al.*, Phys. Plasmas **10**, 1925 (2003).
[9] R. B. Stephens *et al.*, Phys. Rev. Lett. **91**, 185001 (2003).
[10] R. Kodama *et al.*, Nature (London) **418**, 933 (2002).
[11] R. Kodama *et al.*, Nucl. Fusion **44**, S276 (2004).
[12] R. Kodama *et al.*, Nature (London) **432**, 1005 (2004).
[13] Z. L. Chen *et al.*, Phys. Rev. E **71**, 036403 (2005).
[14] Z. L. Chen *et al.*, Phys. Rev. Lett. **96**, 084802 (2006).
[15] R. P. Drake *et al.*, Astrophys. Space Sci. **298**, 49 (2005).
[16] T. Nakamura *et al.*, Phys. Rev. Lett. **93**, 265002 (2004).
[17] M. Koenig *et al.*, Phys. Plasmas **13**, 056504 (2006).
[18] O. L. Landen *et al.*, Rev. Sci. Instrum. **72**, 627 (2001).
[19] H. S. Park *et al.*, Rev. Sci. Instrum. **75**, 4048 (2004).
[20] L. J. Perkins *et al.*, Nucl. Fusion **40**, 1 (2000).
[21] S. Fritzler *et al.*, Appl. Phys. Lett. **83**, 3039 (2003).
[22] J. Rassuchine *et al.*, Med. Phys. **33**, 2251 (2006).
[23] T. Nakamura, H. Sakagami, T. Johzaki, H. Nagatomo, and K. Mima, Phys. Plasmas **14**, 103105 (2007).
[24] S. D. Baton *et al.*, Phys. Plasmas **15**, 042706 (2008).
[25] L. Van Woerkom *et al.*, Phys. Plasmas **15**, 056304 (2008).
[26] J. Rassuchine *et al.*, J. Phys. Conf. Ser. **112**, 022050 (2008).
[27] A. P. L. Robinson and M. Sherlock, Phys. Plasmas **14**, 083105 (2007).
[28] I. M. Frank and V. L. Ginzburg, J. Phys. USSR **9**, 353 (1945).
[29] J. J. Santos *et al.*, Phys. Rev. Lett. **89**, 025001 (2002).
[30] H. A. Sumeruk *et al.* Phys. Plasmas **14**, 062704 (2007).
[31] N. Renard-Le Galloudec, B. I. Cho, J. Osterholz, and T. Ditmire, Rev. Sci. Instrum. **79**, 083506 (2008).
[32] B. I. Cho *et al.*, J. Opt. Soc. Am. B **25**, B50 (2008).
[33] J. Zheng *et al.*, Phys. Plasmas **10**, 2994 (2003).
[34] Y. Sentoku, A. J. Kemp, R. Presura, M. S. Bakeman, and T. E. Cowan, Phys. Plasmas **14**, 122701 (2007).
[35] J. Rassuchine *et al.*, Phys. Rev. E **79**, 036408 (2009).